2016

Thermodynamic Modeling of Screw Expander in a Trilateral Flash Cycle

Hanushan Vasuthevan
Chair of Fluidics, TU Dortmund University, Germany, hanushan.vasuthevan@tu-dortmund.de

Andreas Brümmer
Chair of Fluidics, TU Dortmund University, Germany, andreas.bruemmer@tu-dortmund.de

Thermodynamic Modeling of Screw Expander in a Trilateral Flash Cycle

Hanushan VASUTHEVAN[1]*, Andreas BRÜMMER[2]

[1]TU Dortmund University, Chair of Fluidics
Dortmund, Germany
Phone: +49 231 755 5723, Fax: +49 231 755 5722, E-mail: hanushan.vasuthevan@tu-dortmund.de

[2]TU Dortmund University, Chair of Fluidics,
Dortmund, Germany
Phone: +49 231 755 5720, Fax: +49 231 755 5722, E-mail: andreas.bruemmer@tu-dortmund.de

* Corresponding Author

ABSTRACT

The present paper focuses on the thermodynamic modeling of screw expanders in a trilateral flash cycle. In this process a liquid is pumped from low to high pressure and then heated up close to saturation point. Instead of a vaporous working fluid as usual, a hot liquid is filled in the working chamber of the screw expander. During the filling process the pressure of the liquid drops below the saturation pressure while the temperature remains almost constant due to a fast process. Hence the liquid is in a metastable state. The liquid aspires a stable state and therefore is vaporized during the filling and expansion process due to its increasing chamber volume. Thus a two-phase mixture, vapor and liquid, exists in the working chamber. The simulation presented includes the calculation of fluid states within each chamber to be in thermodynamic equilibrium, which assumes that a sufficient heat transfer exists between the phases to reach a stable state within a time step. Thermodynamic simulations are carried out using water as the working fluid for an exemplary screw expander geometry. The conclusive assessment of the thermodynamic model is demonstrated by the comparison of the simulation results with available experimental measurement results for a corresponding two-phase screw expander.

1. INTRODUCTION

Increasing requirements in compliance with environmental regulations and laws, particularly reduction in CO_2 emissions, lead to concepts to improve the efficiency in energy conversion systems. In modern power plants, in the high power range, combined gas and steam processes are applied to increase efficiency. In this process the steam is heated by the exhaust gases to a temperature of approximately 850 K. Contrarily, efforts are made to increase the efficiency in power recovery from low-temperature heat in the 373 K – 573 K temperature range. Typical examples for low-temperature heat are geothermal sources or industrial waste heat.

The trilateral flash cycle which basically contains liquid heating only and vaporizing during expansion is a means of power recovery for aforementioned low-temperature sources (Smith, 1993). A screw expander is suited for the trilateral flash cycle process as this type of displacement machine is able to expand working fluids with a high liquid content (Kliem, 2002). At the beginning two-phase screw expanders with flash vaporization were essentially examined experimentally. The application of a two-phase screw expander with flash vaporization from a geothermal well was mentioned in a patent for the first time by Sprankle (1973), which was realized with geothermal water for power generation subsequently (Sprankle and McKay, 1974). First experiments of a screw expander in a trilateral flash cycle test rig were carried out by Steidel et al. (1982). In these experiments the flash vaporization with water was realized with a throttle valve on the high pressure side in front of the machine such that a two-phase mixture with a high liquid content enters the screw expander. The maximum measured effective isentropic efficiency was 53%.

First approaches for a theoretical analysis of a two-phase screw expander in comparison to experimental results were made by Taniguchi et al. (1988). For the theoretical analysis a one chamber model was used, which was based on the conservation of mass and energy. In the experiments the screw machine was used as a replacement for a throttle in a heat pump with the aim to increase efficiency and to decrease power consumption of the heat pump. As a working fluid the refrigerant R12 was used. The maximum measured effective isentropic efficiency was 50%. An overview for the development of a trilateral flash cycle system is given by Smith et al. (1993), (1994), and (1996). With thermodynamic cycle simulations the working fluids R12, R113 and n-pentane were examined. For the experimental investigation the working fluid R113 was chosen. The maximum measured effective isentropic efficiency amounts to 70%. Kliem (2005) examined a two-phase screw expander experimentally with a focus on a novel filling system with rotating short nozzles in which hot water was accelerated and injected as a liquid jet in the working chamber. In these tests a maximum effective isentropic efficiency of 55% was measured.

With the evaluation of the available literature it can be said, that there are no detailed methods or models for the design of a two-phase screw expander for a trilateral flash cycle although this technology seems to have a high efficiency potential. A first step in this direction is made with this paper, which presents a method to model a two-phase screw expander. In contrast to the approach of Taniguchi et al. (1988), the conservation of mass and energy in the present work will be derived separately for liquid phase and gas phase. This approach allows a detailed examination of the gas and liquid phase in thermodynamic non-equilibrium. Furthermore detailed heat flow models between phases within working chambers and during leakage flows can be developed and applied on the presented model, which will be realized in future works.

Nevertheless in this paper, as a first step, calculations are done in thermodynamic equilibrium. Taniguchi et al. (1988) and Smith et al. (1996) demonstrated that the assumption of the thermodynamic equilibrium provide acceptable results. The simulations are carried out for an exemplary screw expander geometry, in which a hot liquid is injected through a nozzle, and compared with available experimental results (Kliem, 2005).

2. FUNDAMENTALS

2.1 Trilateral Flash Cycle

The ideal trilateral flash cycle is shown in Figure 1 in a Ts-diagram. The liquid working fluid is pumped isentropic to a higher pressure p_1 and is then heated isobaric to the saturation temperature T_2 related to the pressure p_1. From the saturation point the hot liquid is expanded isentropic within the expander into the wet vapour region to the pressure p_3. Expansion and phase change take place at the same time. Depending on boundary conditions the phase change can occur explosively which is referred to as flash vaporization. The cycle is closed with condensation of the two-phase mixture.

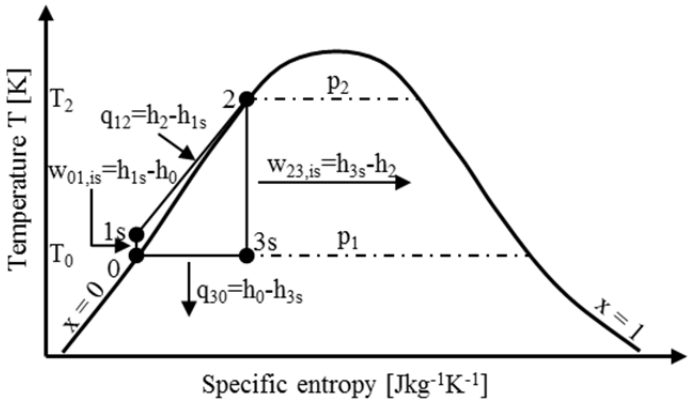

Figure 1: Ts-diagram of the ideal trilateral flash cycle

2.2 Screw Expanders

Screw expanders are rotary displacement machines with spiral shaped intermeshing rotors enclosed in a housing. The gaps of the rotors with the enclosed housing form the working chambers. The periodical change of the working chamber volume in a working cycle takes place due to the rotation of the rotors. Figure 2 qualitatively presents the progression of the chamber volume as well as the inlet and the outlet area as functions of the phase angle for one working chamber of a screw expander. A phase angle of $\varphi = 1$ is equal to the tooth pitch angle of the male rotor

which depends on the number of lobes. The working cycle is divided into three steps. The first step is the filling process, in which the working chamber is filled with the working fluid from the high pressure side while the volume increases. With further rotation the rotor edges passes the control edges which are within the housing. At this moment the connection between the high pressure side and the working chamber over the inlet area is separated. The filling process ends and the working chamber -except of clearances- is enclosed from the environment. At this moment the expansion process begins at the theoretical expansion volume $V_{ex,th}$. The expansion process proceeds with further rotating of the rotors while pressure and temperature drops. This process ends when the working chamber reaches the control edge on the low pressure side at its maximum chamber volume V_{max}. The working chamber is then connected to the low pressure side through the outlet area. At this point the discharge of the working fluid begins while the chamber volume decreases, which is the third step of the working cycle. The working cycle ends with the disappearing of the chamber volume.

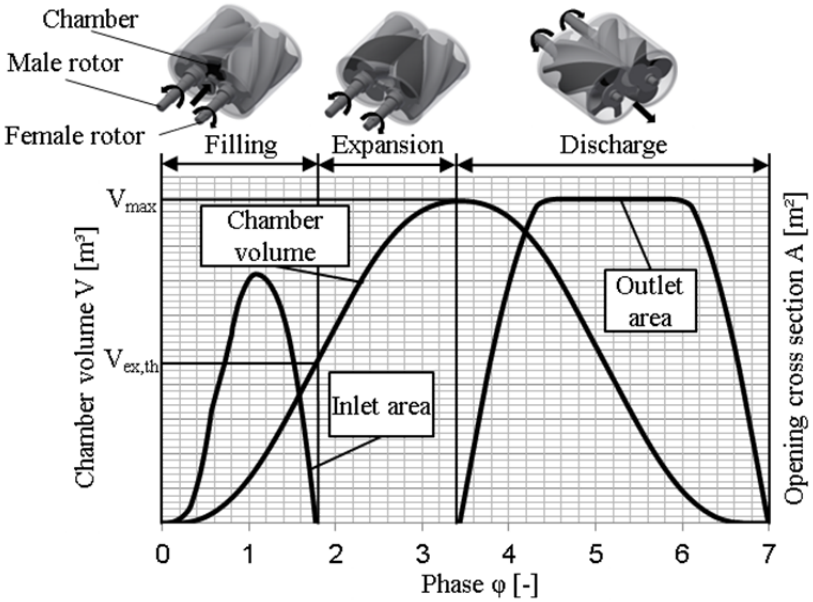

Figure 2: Volume curve and chamber openings for a workings cycle of a screw expander

For a given screw expander geometry with a maximum chamber volume the initiation of the theoretical expansion depends on the internal volume ratio v_i which is defined in equation (1). Thus the internal volume ratio affects the inlet area of a screw expander. The inlet area decreases with increasing internal volume ratio.

$$v_i = \frac{V_{max}}{V_{ex,th}} \tag{1}$$

3. SIMULATION PROCEDURE AND THERMODYNAMIC MODELLING

In this chapter the procedure of the simulation and its thermodynamic modelling are described. The simulation tool used for a multi-chamber model is mainly based on Janicki (2007). The essential requirement for the simulation is a multi-chamber model that presents the geometrical description of the angle dependent chamber volumes and gap areas between chambers. Every working chamber and its connections over gap areas are calculated simultaneously within one tooth pitch angle of the male rotor. The calculations are mainly based on the conservation of mass and energy which are considered separately for each phases. This approach offers the option to consider thermodynamic non-equilibrium states within working chambers.

3.1 Conservation of mass

In equation (2) and equation (3) the conservation of mass for each phase is shown. The change of the mass over time in a gas or liquid control volume depends on the mass flow over the surface of the control volumes including the phase changes. The function $\dot{m}_{phase}$ describes the mass flow which vaporizes or condenses from the corresponding phase. If $\dot{m}_{phase}$ is a positive value the mass flow is vaporized from the liquid phase which is subtracted from the

liquid mass flow and added to the gas mass flow. Vice Versa if $\dot{m}_{phase}$ is a negative value the mass flow condenses from the gas phase.

$$\frac{dm_G}{dt} = \sum_f (\dot{m}_G) + \dot{m}_{phase} \tag{2}$$

$$\frac{dm_L}{dt} = \sum_f (\dot{m}_L) - \dot{m}_{phase} \tag{3}$$

3.2 Conservation of energy

The conservation of energy for the gas and liquid phase is shown in equation (4) and equation (5). The left-hand-side of equation (4) and equation (5) is the change of the energy in the control volume over the time of the gas phase and liquid phase. It is assumed that kinetic and potential energy due to the gravitation can be neglected in the control volumes. Hence, only the internal energy will be considered in the control volumes.
On the right-hand-side of equation (4) and equation (5) the energy flows over the control volume surfaces are described. The terms $\dot{Q}_{SG}$ and $\dot{Q}_{SL}$ are the heat flow between a solid part and the gas or liquid phase. The heat flow between the phases is described with $\dot{Q}_{LG}$. It is assumed that the pressure-volume work of the whole chamber W_{Ch} is only performed by the gas phase and not from the liquid phase. The calculation of the pressure-volume work W_{Ch} by means of equation (6) includes the change of the whole chamber volume over time, which depends on the volume curve of the geometry. Independent of the pressure-volume work of the whole chamber the control volume of the gas phase can be deformed due to a volume change of the liquid. The volume of the liquid can be considered as incompressible and occupy the whole chamber volume in parts. If the control volume of the gas phase is deformed by the liquid phase to a smaller volume, pressure-volume work W_L is performed on the gas phase. This energy is taken from the liquid phase because the control volume of the gas phase is reduced by the liquid phase. All inlet and outlet total-enthalpy flows over the control volume surfaces of each phase are described by the summation of $\dot{m}_G h_{t,G}$ and $\dot{m}_L h_{t,L}$. The total enthalpy is that of the upstream state point of the flow. That means if the flow is into the control volume, the total-enthalpy is from the chamber the mass flow came from. If the flow is out of the control volume, the total-enthalpy is that of the considered control volume.

$$\frac{dE_G}{dt} = \dot{Q}_{SG} + \dot{Q}_{LG} + \frac{dW_{Ch}}{dt} - \frac{dW_L}{dt} + \sum_f \dot{m}_G h_{t,G} \tag{4}$$

$$\frac{dE_L}{dt} = \dot{Q}_{SL} - \dot{Q}_{LG} + \frac{dW_L}{dt} + \sum_f \dot{m}_L h_{t,L} \tag{5}$$

$$\frac{dW_{Ch}}{dt} = -p\frac{dV_{Ch}}{dt} \tag{6}$$

3.3 Chamber filling

The filling process is the flow from the high pressure side into a chamber volume. It is assumed that the working chamber is filled with a hot liquid over an injector nozzle instead of a conventional inlet area to improve flash vaporization of the fluid in the working chamber. The calculation of the mass flow rate is carried out with the Bernoulli equation for unsteady and incompressible flows from point 1 (reservoir upstream of the nozzle) to point 2 (outlet of the nozzle) along a streamline s, which is given in equation (7) neglecting the geodetic height differences between 1 and 2 and friction losses.

$$\frac{p_1}{\rho} + \frac{c_1^2(t)}{2} = \frac{p_2(t)}{\rho} + \frac{c_{2s}^2(t)}{2} + \int_1^2 \frac{\partial c(s,t)}{\partial t} ds \tag{7}$$

Point 1 can be a reservoir where the kinetic energy can be neglected and point 2 is the position at the nozzle outlet. At point 2 the pressure p_2 is assumed to be equal to the pressure of the working chamber which is to be filled. The pressure of the working chamber changes dependently on rotor angle or time.
The conversation of mass for a streamline from point 1 to point 2 is given in equation (8).

$$c(s,t) \cdot A(s) = c_{2s}(t) \cdot A_2(t) \tag{8}$$

With the assumption that the outlet area A_2 is constant and time-independent, equation (8) can be differentiated with respect to the time and integrated along the streamline, which yields to equation (9)

$$\int_1^2 \frac{\partial c(s,t)}{\partial t} ds = \frac{dc_{2s}(t)}{dt} \int_1^2 \frac{A_2}{A(s)} ds \tag{9}$$

Combining equation (7) and (9) yields to the following differential equation (10) with the stationary velocity $c_{stat,2}$, which is depending on the time-dependent pressure difference between point 1 and the filled working chamber:

$$\frac{dc_{2s}(t)}{dt} = \left(\frac{c_{stat,2s}^2(t)}{2} - \frac{c_{2s}^2(t)}{2} \right) \cdot \frac{1}{\int_1^2 \frac{A_2}{A(s)} ds} \tag{10}$$

The solution of the differential equation (10) for a constant and time-independent steady state velocity $c_{stat,2s}$ is given in equation (11). The time-dependent velocity $c_{2s}(t)$ is a hyperbolic tangent function which will lead to the stationary velocity $c_{stat,2s}$ for infinite time. The parameter D is determined by the initial condition and is zero for $c_{2,s}(0) = 0$. Furthermore the velocity at the nozzle outlet is depending on the geometry along the streamline.

$$c_{2s}(t) = c_{stat,2s} \cdot \tanh \left(\frac{c_{stat,2s} \cdot (D \int_1^2 \frac{A_2}{A(s)} ds + t)}{2 \int_1^2 \frac{A_2}{A(s)} ds} \right) \tag{11}$$

During the filling process the steady state velocity $c_{stat,2s}$ changes at the nozzle outlet which is not considered in the solution of equation (11). In the simulation the changeable steady state velocity at the nozzle outlet will be applied in equation (11), which is an approximation.
With equation (11) the theoretical maximum mass flow rate of the liquid is determined with the density ρ and the nozzle exit area A_2. Due to losses along the streamline the actual mass flow rate will be smaller. Therefore the losses are considered with a time dependent flow coefficient α(t). The actual mass flow rate $\dot{m}_L(t)$ for the filling of the working chamber is given in equation (12).

$$\dot{m}_L(t) = \alpha(t) \dot{m}_{th}(t) = \alpha(t) \rho A_2(t) c_{2,s}(t) \tag{12}$$

3.4 Leakage Calculation

For the calculation of the leakages a homogenous distribution of the two-phase mixture in the working chamber is assumed. This is a simplification as the leakage flow is essentially depending on the amount of liquid in the working chamber due to its sealing properties concerning the gap flows. Furthermore the gap flow is calculated in thermodynamic equilibrium which is also a simplification.
In Figure 3 an exemplary situation of a housing gap flow is shown. The calculation of the velocity from a chamber volume in the gap plane is done with the conservation of energy. At position 1 (chamber) the state is known. For the position in the gap plane it is assumed that the pressure p_{gap} equals to the pressure p_2 of the underlying working chamber. Furthermore assuming isentropic flow from chamber 1 to the gap plane the fluid state in the gap plane is known too.

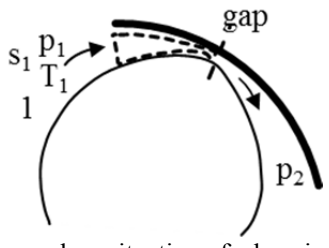

Figure 3: Exemplary situation of a housing gap flow

By means of the conservation of energy the isentropic velocity $c_{gap,s}$ in the gap plane is calculated with equation (13). The enthalpy in equation (13) is determined in thermodynamic equilibrium for the two-phase mixture.

Furthermore it is assumed that the velocity from the gas and liquid is equal in the gap plane. In the gap plane the vapor content x_{gap} will be evaluated in thermodynamic equilibrium to determine the liquid and gas mass flow as shown in equation (14) and equation (15). The calculated gas mass flow in the gap plane, which is inserted in chamber 2, is not equal to the change of gas mass within chamber 1, because during the flow between chamber 1 and the gap plane, phase change occurs. This also applies for the liquid mass flow. The gas and liquid mass taken out of the chamber 1 must be calculated with the vapor content x_1 in chamber 1. This must be taken into account by use of the conservation of mass and energy.

$$c_{gap,s} = \sqrt{2 \cdot \left(h_1(p_1, s_1) - h_{gap,s}(p_2, s_1)\right)} \tag{13}$$

$$\dot{m}_{G,s} = \dot{m}_{gap,s} x_{gap} = c_{gap,s} \rho_{gap} A_{gap} x_{gap} \tag{14}$$

$$\dot{m}_{L,s} = \dot{m}_{gap,s}(1 - x_{gap}) = c_{gap,s} \rho_{gap} A_{gap}(1 - x_{gap}) \tag{15}$$

Due to the assumption that the pressure in the gap plane equals the underlying working chamber, a choked flow may occur. This has to be checked by calculation of the critical pressure $p_{gap,crit}$. If the pressure p_2 is smaller than the pressure $p_{gap,crit}$ the assumed mass flux in the gap plane equals the maximum mass flux is $(\rho c)_{crit}$, as shown qualitatively in Figure 4.

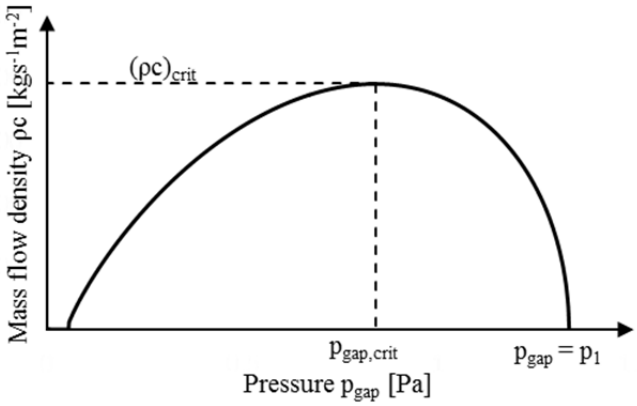

Figure 4: Mass flux depending on pressure $p_2 = p_{gap}$ for constant pressure p_1

The calculation of the critical mass flux is done iteratively by varying the pressure p_{gap} for constant pressure p_1. The criterion for the critical mass flux in the gap plane is given in equation (16). To limit the required calculation time for the iteration the first step is to calculate the derivative of the mass flux at the known pressure p_2. If the gradient is negative the flow is subcritical and the determination of the critical mass flux is not necessary.

$$\left(\frac{d(\rho c)}{dp}\right)_{gap} = 0 \tag{16}$$

Furthermore losses have to be considered and thereby the calculation of the actual mass flow rate can be treated in the same way as for the filling process with a flow coefficient as shown in equation (12).

3.5 Solution Procedure

For a given time step or rotor angle which is dependent on the angular frequency the geometry will be considered as a frozen model. It therefore follows, that chamber volumes and gap areas between chambers are defined. The basic simulation steps for this frozen model are shown in Figure 5. The first step is the calculation of the pressure-volume work due to the volume change compared to the time step before. The second step is the calculation and the transfer of heat flows between phases in a chamber volume. Thermodynamic equilibrium can be assumed if a sufficient heat transfer exists to reach the stationary stable state. Then the state can be calculated directly by means of an equation of state. Another approach is to calculate the heat flows with suitable heat transfer and vaporization models with consideration of the distribution of liquid and gas in the chamber which is not considered and not used here but scheduled for future work. In the present calculations the fluid states within the chambers are calculated in thermodynamic equilibrium. The last step is the calculation and the exchange of mass and energy due to fluid flows

(gap, filling, discharge flows and phase changes) and heat flows (between solid parts and fluid). Subsequently the next time step can be calculated. The steps are performed successively within a small time increment to minimize the error. The calculation of all time steps in a working cycle is referred to as iteration. The stationary solution is achieved when the deviation of mass and energy in all time steps and all chamber volumes between two iterations is lower than a predefined deviation.

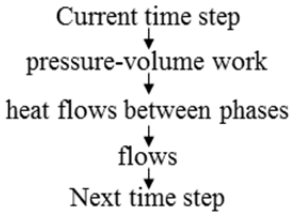

Figure 5: Calculation procedure within a time step

4. COMPARISON OF SIMULATION AND EXPERIMENTAL RESULTS

Kliem (2005) examined a two-phase screw expander with a novel filling system in a trilateral flash cycle with the working fluid water. The filling system consists of a disk with short nozzles, which is fixed on the high pressure side of the female rotor. The inlet nozzles are located in the middle of the tooth space area. In the housing an inlet segment (elongated hole) is built in which has got a permanent connection to the high pressure side. During a specific rotating angle the nozzles passes the inlet segment and a connection exists between the high pressure side and a nozzle. In this configuration a working chamber will be filled and the hot liquid will be vaporized in the chamber.
In the experimental investigation flow coefficients were measured depending on the rotor angle for steady state flow conditions without the machine. Furthermore a pressure indication of the expander was performed.

4.1 Data of Geometry and Simulation

In Table (1) data of geometry and simulation are presented. The gap heights of the screw expander are estimated because these are unknown. Furthermore the fluid states per chamber are calculated in thermodynamic equilibrium and no heat transfer between solid parts and fluid is considered (adiabatic). The flow coefficient for all gaps are set constant to $\alpha = 0.8$ neglecting the influence of the rotor speed. For the filling system measured flow coefficients are used which are depending on the rotor angle. The geometric parameter for the unsteady flow of the filling system is estimated rudely from the available data due to lack of detailed information of the geometrical dimension of the flow path.

Table 1: Geometry and Simulation Data

Geometry and simulation data	
Rotor profile	Asymmetric SRM profile
Number of lobes – male/female	5 / 7
Crown circle – male/female	0,166 m / 0,154 m
Maximum chamber volume	$6{,}64 \cdot 10^{-4}$ m^3
Internal volume ratio	4,1
Profile gap height	$5 \cdot 10^{-5}$ m
Front gap height/ housing gap height	$8 \cdot 10^{-5}$ m
Heat flow model between phases	Thermodynamic equilibrium
Flow coefficient gap	0,8
Flow coefficient filling	Flow coefficients measured for steady state flow conditions by Kliem (2005)
Geometry parameter – filling: $\int_1^2 \frac{1}{A(s)} ds$	500 m^{-1}

4.2 Mass Flow Rate

In the experiment the mass flow rate was measured on the high pressure side in front of the machine. Due to the relative rotation between the rotating disk and the inlet segment a gap exists which results to a leakage mass flow.

This leakage flow is not considered in the simulation. Therefore it is to be expected that the simulated mass flow rate is lower than the measured mass flow rate. In Figure (6) the mass flow rate of simulation and experiment are presented depending on the male rotor circumferential speed for different inlet temperatures with corresponding inlet pressures. The symbols are measured points from the experiment and the curves are the results from the simulation.

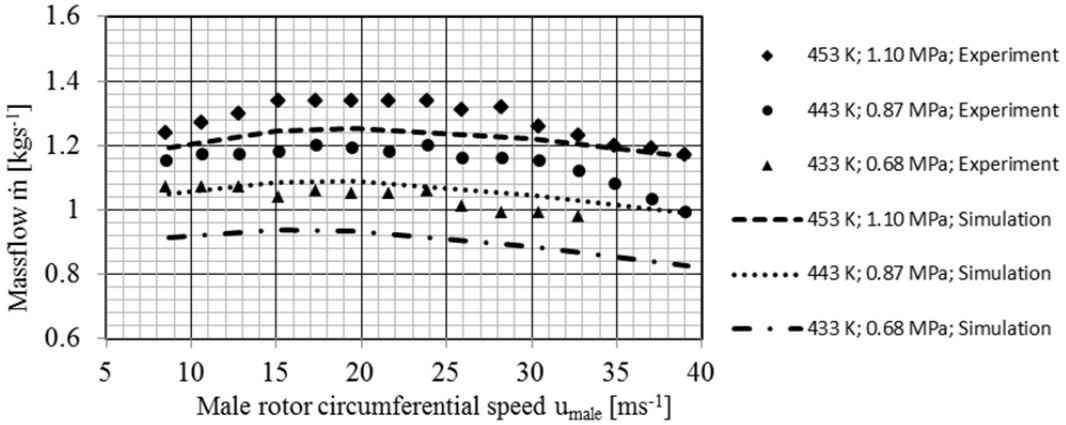

Figure 6: Mass flow rate depending on the male rotor circumferential speed

The mass flow rate has got a minor dependency of the circumferential speed. For high inlet temperatures a maximum of the mass flow rate can be identified which is decreasing with further circumferential speed. The reason for the decreasing mass flow rate is the unsteady filling. The liquid has got to be accelerated once a connection to the nozzle exists and does not reach the steady state velocity within the filling phase at high circumferential speed.
The mass flow rates of the simulation are smaller than measured values due to the leakage mass flow between the inlet segment and the rotating disk as expected. The deviation can be interpreted as an additional not simulated leakage. With increasing circumferential speed the deviation between simulation and experiment decreases. A possible reason for this is a higher unsteady loss mechanism with increasing circumferential speed which decreases the mass flow rate in the experiment. Another reason is that the additional not simulated leakage mass flow rate in the experiment is decreasing with increasing circumferential speed.

4.3 Internal Work and Indicator Diagrams

In Figure (7) the internal work (pressure-volume work of working cycle) depending on the male rotor circumferential speed is shown. The symbols are measured points from the experiment and the curves represent the simulation results. The internal work is calculated from the indicator diagrams. The simulation provides an acceptable estimation of the internal work. The maximum deviation for the examined range is 17,5% at a temperature of 453K and a circumferential speed $u_{male} = 13{,}9\ ms^{-1}$.
A closer examination can be done with an indicator diagram. In Figure (8) the indicator diagrams for a temperature of 453K and three circumferential speeds are shown. For a circumferential speed of $u_{male} = 8{,}71\ ms^{-1}$ the pressure of the simulation decreases during the filling while the pressure of the experiment is nearly constant. It is assumed that the pressure decreases due to the simplified simulation of the leakage flow. In the real case there is the possibility that leakages are sealed with the liquid phase.
For a higher circumferential speed of $u_{male} = 19{,}6\ ms^{-1}$ the time for the leakage flow is reduced such that the pressure of the simulation during the filling stays nearly constant. During the expansion process the pressure of the simulation decreases faster than the pressure of the experiment. The reason for this is again the modeling of the leakage flow whereby sealing effects of gaps and distribution of the liquid phase or the gas phase in the chamber are not considered. With increasing circumferential speed the stationary velocity during the filling cannot be reached. The pressure of the simulation at the circumferential speed $u_{male} = 39{,}2\ ms^{-1}$ does not reach the pressure of the experiment during the beginning of the filling. A possible reason is that the approximation for the calculation of the chamber filling at higher circumferential speed is inaccurate. In the expansion phase the curve progression of simulation and experimental are nearly identical. At this circumferential speed the impact of the leakage flow seems to be minor.

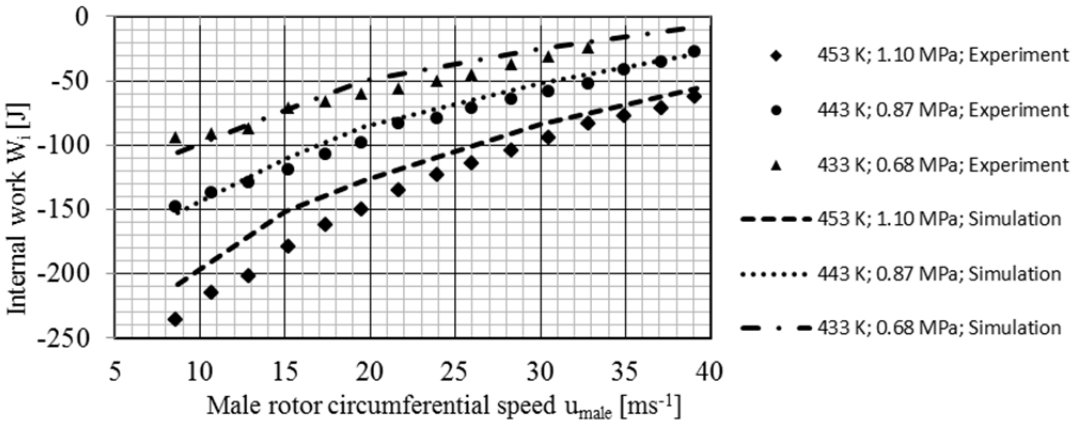

Figure 7: Internal work depending on the male rotor circumferential speed

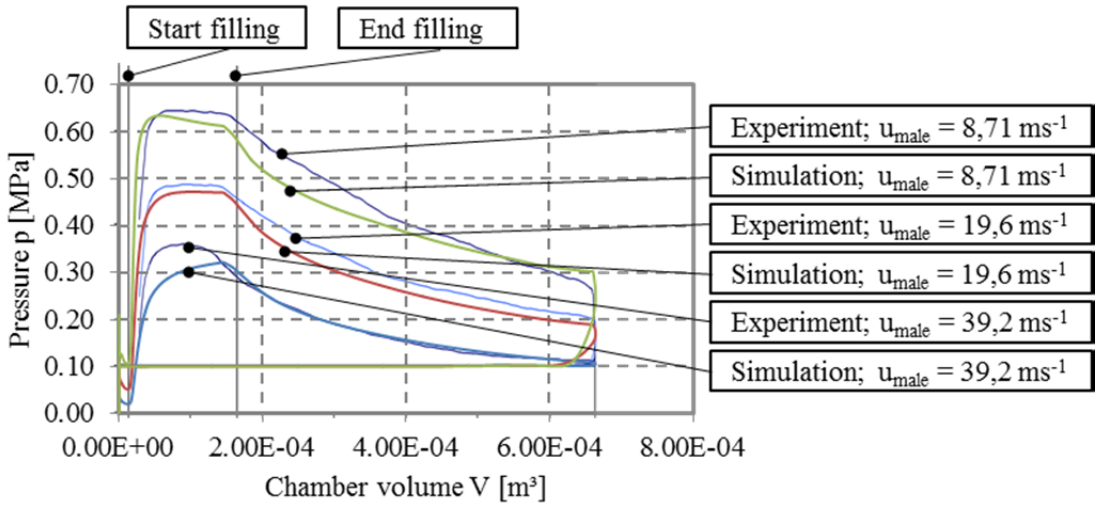

Figure 8: Indicator diagrams for different circumferential speeds at T_{inlet} = 453K and p_{inlet} = 1,1MPa

6. CONCLUSIONS

The presented simulation model to calculate a screw expander with hot liquid injection and flash vaporization is an acceptable approach for a first estimation of mass flow and internal power. This is validated by comparison of simulation and experimental results. A potential reason for existing deviations between simulation and experiment is the assumption of the thermodynamic equilibrium for the calculation of chamber states and gap flows.
Consideration of a detailed atomization and vaporization model for the filling process may improve the simulation model. Additionally a model of the distribution of liquid and gas within the chambers is required in order to model more realistic gap flows.

NOMENCLATURE

A	cross section	(m²)
c	velocity	(m/s)
h	specific enthalpy	(J/kg)
$\dot{m}$	mass flow	(kg/s)
p	pressure	(Pa)
$\dot{Q}$	heat flow	(J)

t	time	(s)
T	temperature	(K)
u	circumferential speed	(m/s)
v_i	internal volume ratio	(-)
V	volume	(m^3)
W	work	(J)
x	vapor content	(-)
α	flow coefficient	(-)
ρ	density	(kg/m^3)
φ	phase	(-)

Subscript

ch	chamber
crit	critical
ex	expansion
G	gas
L	liquid
max	maximum
S	solid
s	isentropic
stat	stationary

REFERENCES

Janicki, M., (2007), *Modellierung und Simulation von Rotationsverdrängermaschinen*, Dissertation, Universität Dortmund

Kliem, B., (2002), The Two-Phase Screw-Type Engine with Flash Evaporation, *Schraubenmaschinen 2002 VDI-Berichte 1715*, Düsseldorf, VDI Verlag, 167-177

Kliem, B., (2005), *Fundamentals of the Two-Phase Screw-Type Engine*, Dissertation, Universität Dortmund

Smith, I. K., (1993), Development of the trilateral flash cycle system: Part 1: fundamental considerations, *Journal of Power and Energy*, 207(3),179 – 194.

Smith, I. K., Marques da Silva, R.P., (1994), Development of the trilateral flash cycle system: Part 2: increasing power output with working fluid, *Journal of Power and Energy*, 208(2),135-144.

Smith, I. K., Stosic, N., Aldis, C. A., (1996), Development of the trilateral flash cycle system: Part 3: the design of high-efficiency two-phase screw expanders, *Journal of Power and Energy*, 210(1), 75-93.

Sprankle, R. S.,(1973), *Electrical Power Generating System*, patent specification, United States, publication number: 3,751,673

Sprankle, R. S., McKay, R.A., (1974), *Experience, Plans, and a Mixed Flow Expander*, Hydrothermal Power, Ltd, California, Pasadena

Steidel, R. F., Weiss, H., Flower, J.E., (1982), Performance characteristics of the Lysholm engine as tested for geothermal power applications in the Imperial Valley, *Journal of Engineering for Power,*104(1), 231-240

Taniguchi, H., Kudo, K., Giedt, W. H., Park, I., Kumazawa S., (1988), Analytical and experimental investigation of two-phase flow screw expanders for power generation, *Journal of Engineering for Gas Turbines and Power,*110(4), 628-635